ELSEVIER

Polymer 40 (1999) 7147–7156

polymer

Influence of casting solvents on microphase-separated structures of poly(2-vinylpyridine)-*block*-polyisoprene

Y. Funaki[a], K. Kumano[a], T. Nakao[a], H. Jinnai[a], H. Yoshida[a], K. Kimishima[a], K. Tsutsumi[a], Y. Hirokawa[a], T. Hashimoto[a,b,*]

[a]*Hashimoto Polymer Phasing Project, ERATO, Japan Science and Technology Corporation, 15 Shimogamo-morimoto, Kyoto 606-0805, Japan*
[b]*Department of Polymer Chemistry, Graduate School of Engineering, Kyoto University, Sakyo-Ku, Yoshida-honmachi, Kyoto 606-8501, Japan*

Received 5 November 1998; received in revised form 21 January 1999; accepted 1 February 1999

Abstract

Influences of casting solvent on the microphase-separated structures of poly(2-vinylpyridine)-*block*-polyisoprene films were studied by transmission electron microscopy and small-angle X-ray scattering. The variations of the structures obtained were consequences of vitrification of microdomain structures developed during the solvent casting processes. The various microphase-separated structures were properly understood by considering the Hansen's solubility parameters of the solvent and the copolymer, which quantify the polymer–solvent interactions in the system.

Keywords: Poly(2-vinylpyridine)-*block*-polyisoprene; Casting solvent; Microphase-separated structures

1. Introduction

Diblock copolymers composed of two segregating blocks are well known to phase-separate into microdomain structures, such as spherical, cylindrical, and lamellar microdomains, and also into various bicontinuous structures, in bulk [1–5] and in concentrated solutions [1,6–10]. Since 1960s, both static and dynamic phenomena of the microphase separations have been under comprehensive experimental and theoretical investigations mainly due to those interesting structures. On account of these studies, equilibrium structures can now be predicted to certain extent in terms of various field theories [11–19]. However, an actual diblock copolymer film prepared from solution by solvent casting method often present nonequilibrium natures [20,21]. The bulk microphase-separated structures of the as-cast films depend upon the solvents used in the casting processes. The structures are often found to be considerably different from those predicted by the equilibrium theory.

In spite of the importance of the structural formation in the diblock copolymer films in both scientific and technological applications, less attention has been paid to the effect of the casting process on the morphologies. Only several systematic studies have been reported [10,20,22–26]. One of the pioneering works was performed by Inoue et al. [23,24], in which they have shown that the structures of diblock copolymer films composed of polystyrene (PS) and polyisoprene (PI) vary from spherical to lamellar microstructures depending on the solvent used in the casting processes. Later, Cohen and Bates have also reported the influence of the casting processes on the morphologies of the block copolymer films composed of PI and poly(*n*-butyl methacrylate) [25]. They have shown that a rate of solvent evaporation as well as the nature of a solvent influenced the microphase-separated structures. These results indicate that the bulk structures of diblock copolymer films obtained after complete solvent evaporation are strongly influenced by the microphase-separated structures developed in the solutions. During the casting process, concentration of the polymer, ϕ_p, gradually increases, and at a critical concentration (about 10%) the system starts phase-separating into microdomains [8,9,27]. Once the microphase separation has been developed, nature of the solvent influences the degree of the swelling of the polymer chains in each domain and hence an effective volume fraction of each domain. A neutral solvent should be equally distributed into the both microdomains, resulting in swelling both of the blocks to the same extent. On the other hand, even a slight degree of the solvent selectivity can lead to a preferential swelling of one of the domains, as reported by Lodge et al. [28].

In the present report we will discuss the influence of the solvents used in the casting processes on the internal

* Corresponding author.

0032-3861/99/$ - see front matter
PII: S0032-3861(99)00112-3

Table 1
Properties of the diblock copolymers used and their equilibrium microphase-separated structures

Sample	f_{P2VP}[a]	Molecular weight $M_n \times 10^3$			M_w/M_n	Expected equilibrium morphology
		P2VP[b] block	PI block	Total		
P2VP-b-PI(26/74)	0.26	8.1	18.8	26.9	1.16	Hexagonal cylinder
P2VP-b-PI(12/88)	0.12	3.4	21.0	24.5	1.24	bcc sphere

[a] Volume fractions of the block copolymers were calculated adapting the densities of PI and P2VP to be 0.913 and 1.14 glcm^3, respectively.
[b] The glass transition temperature of P2VP is ca. 104°C [50].

structures of the solvent-cast films based on the information obtained by a small angle X-ray scattering (SAXS) method and transmission electron microscopy (TEM). In the previous studies [23–27], the classical solubility parameters which only take the London dispersion force into consideration (Hildebrand solubility parameter) were used. However, solvents normally have permanent dipole, and thus it is essential to consider polymer–solvent interaction not only from the dispersion force but also from dipole–dipole interaction. Besides, hydrogen bond may sometimes play a significant role in formation of microphase-separated structures. All these interactions have to be considered in order to clearly discuss the solvent selectivity against the polymer chains. In the current work, we introduced the Hansen's solubility parameters that incorporate the dipole–dipole and the hydrogen bonding interactions (see Section 3.3 for details), which successfully explains the solvent selectivity and thus formation of the microphase-separated structures.

The block copolymers employed in the experiments are composed of PI and poly(2-vinylpyridine) (P2VP). The segregation between PI and P2VP is considerably large compared with that between PI and PS, which are the standard components of the block copolymers widely used for many block copolymer related investigations. This feature may allow us to investigate the influence of a solvent quality on the microphase-separated structure in the as-cast films by applying variety of solvents possessing a wide range of solubility parameters.

2. Experimental

2.1. Diblock copolymer synthesis

Poly(2-vinylpyridine)-*block*-polyisoprene diblock copolymers (P2VP-b-PI) having different compositions were synthesized by the sequential living anionic polymerization [29]. First, isoprene was polymerized by using *sec*-butyllithium (Aldrich, cyclohexane solution) as an initiator in dried THF at 0°C under nitrogen atmosphere. For the characterization of the molecular weight of the polyisoprene block, an aliquot part of the polymerization solution was taken out by a syringe and analyzed by gel permeation chromatography (GPC) using Tosoh HLC8020 with TSK gel columns ($G2500H_{XL}$ + $G4000H_{XL}$ + $G6000H_{XL}$). The calibration curve of standard polyisoprene (Polymer Standards Services) was used to determine the molecular weight and its distribution. Next, 2-vinylpyridine, dried over calcium hydride and distilled under reduced pressure just before the polymerization, was added to the residual THF solutions at 0°C by a syringe for the living anionic polymerization of poly(2-vinylpyridine) block chains. The living anions of the polyisoprene and the block copolymers were quenched with dried methanol. The polymers were collected by the precipitation into a large excess of methanol, and purified by reprecipitation and freeze-drying.

The diblock copolymers thus obtained were characterized by the GPC. *N*,*N*,*N*′,*N*′-tetramethylethylenediamine was added to the eluent (chloroform) by 5% in volume to avoid the adsorption of P2VP on polystyrene gels. The calibration curve of standard polystyrene (Tosoh) was used to determine the apparent molecular weight and its distribution. The molecular compositions of the block copolymers were determined by proton nuclear magnetic resonance spectroscopy (^{1}HNMR, JEOL EX400). The volume fractions of the P2VP block, f_{P2VP}, were calculated by using the densities 0.913 [30] and 1.14 [31] for PI and P2VP, respectively. All estimated values are shown in Table 1.

2.2. Preparation of film specimens

Film specimens were prepared by solvent casting method as follows: The well-dried diblock copolymer was dissolved into 5 wt.% solution using dry solvent and put into a Teflon petri dish (33 mm in diameter). Then the petri dish was placed into a moisture-free environment at 28°C. Evaporation of the solvent was proceeded gradually and it took about 4 days for the complete evaporation. The polymer film thus obtained was about 0.5 mm in thickness. We have employed seven different solvents for casting, which have different solvent quality against PI and P2VP blocks: *n*-butylchloride (*n*-BtCl), tetrachloromethane (CCl_4), toluene, benzene, tetrahydrofuran (THF), dichloromethane (CH_2Cl_2) and 1,4-dioxane. Special attention was paid to isolate each of the petri dishes containing different solvents to avoid mixing the evaporated solvent gases during the casting processes. The films thus obtained were then dried

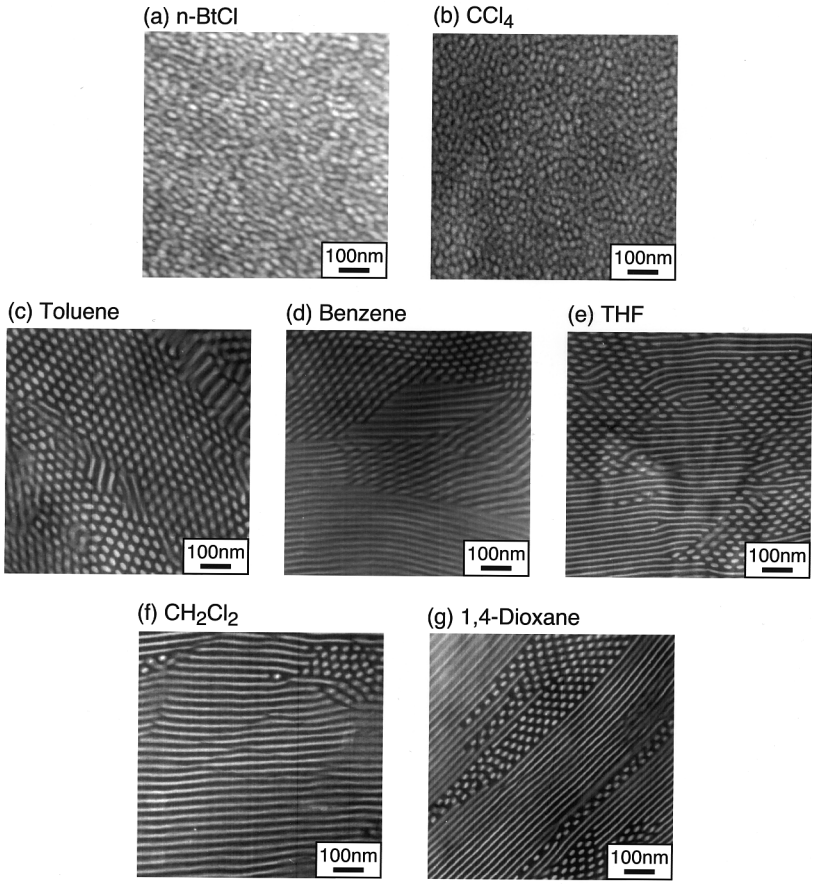

Fig. 1. Transmission electron micrographs of thin sections of the P2VP-b-PI(26/74) diblock copolymer films prepared by solvent casting from (a) *n*-BtCl, (b) CCl_4, (c) toluene, (d) benzene (e) THF, (f) CH_2Cl_2 and (g) 1,4-dioxane solutions. The as-cast sample films were annealed at 140°C for 12 h before the observations. The sample films were stained with OsO_4. Thus the dark and bright regions seen in the micrographs are PI and P2VP phases, respectively.

under vacuum for 24 h and annealed at 140°C for 12 h before structural analysis.

We have also carried out the structural analysis of the solutions at various ϕ_p. The samples used for this series of the experiments were prepared by dissolving the diblock copolymer in 1,4-dioxane. The solutions were kept for 12 h at 50°C in sealed bottles before use. ϕ_p of the solutions were determined by measuring their weights after the SAXS analysis and the total polymer weights after evaporating the solvent.

2.3. TEM observation

For TEM observation, an unstained small pieces of the film sample was embedded in epoxy resin, which was hardened at 60°C for about an hour. After trimming the specimen, it was microtomed to the ultrathin sections of about 50 nm thickness using a Reichert Ultracut S with a cryochamber FCS operated at −110°C. The sections were exposed to osmium tetraoxide (OsO_4) vapor for about half-an-hour to selectively stain PI domain. The microphase-separated structures in the sections thus obtained were observed by TEM (JEOL, JEM-2000FXZ) operated at 200 kV.

2.4. SAXS measurement

SAXS measurements were conducted with an apparatus consisting of an 18 kW rotating-anode X-ray generator (M18XHF-SRA, MAC Science Co. Ltd., Yokohama, Japan) with a graphite crystal monochromator, a three-slit collimator, a vacuum path for incident and scattered beams, and a one-dimensional position sensitive proportional counter (PSPC). The sample-to-detector distance was about 1.8 m. A CuKα line beam monochromatized with a graphite crystal with a wavelength of 0.1542 nm was used. Measurements were carried out under the conditions of the incident X-ray beam being parallel to the surface of the stacked film sample and direction of the detector being perpendicular to the film surface (edge view) at room temperature. Typical measurement time for one sample was 2 h. The SAXS profiles were corrected for the absorption of the sample, background scattering, smearing due to the slit-height and slit-width (desmearing), and the

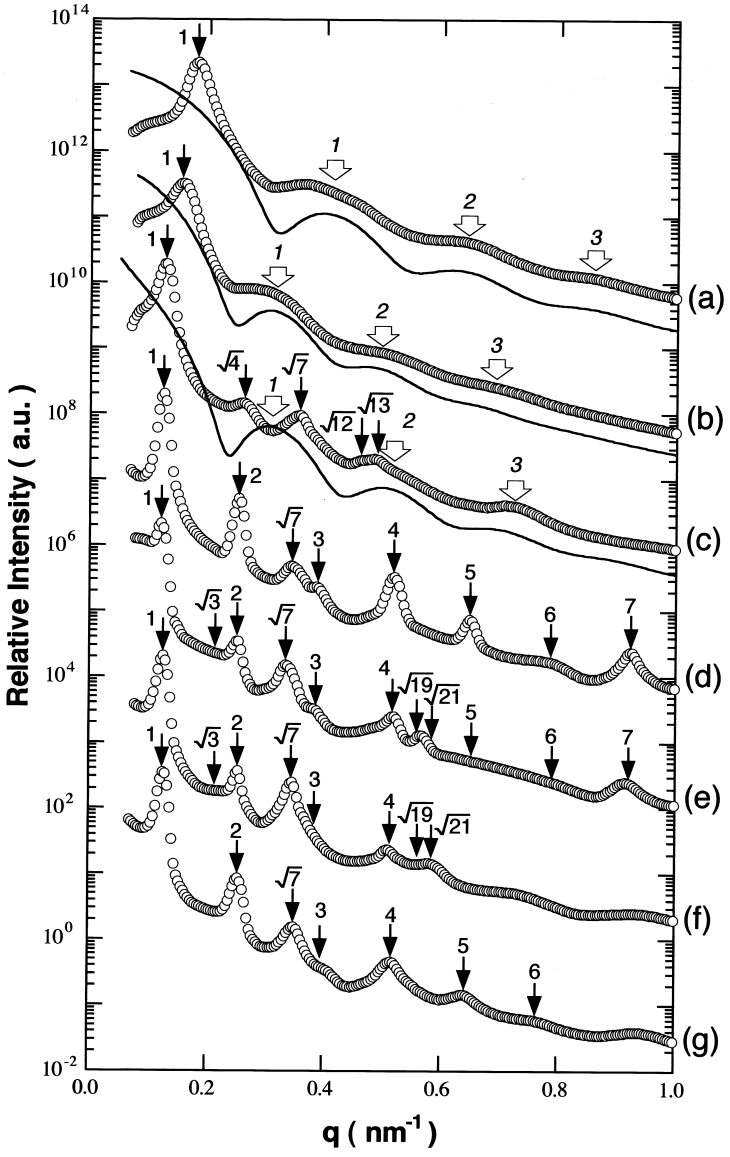

Fig. 2. SAXS profiles of P2VP-b-PI(26/74) diblock copolymers prepared by casting from (a) *n*-BtCl, (b) CCl_4, (c) toluene, (d) benzene (e) THF, (f) CH_2Cl_2 and (g) 1,4-dioxane solutions. The as-cast films were annealed at 140°C for 12 h before the measurements. The solid lines plotted under the profiles (a) and (b) are theoretically calculated from form for spheres. Radii (r) of the spheres and their standard deviations (σ_r) used for the fits are (a) $r = 13.9$ nm, $\sigma_r = 1.3$ nm and (b) $r = 17.8$ nm, $\sigma_r = 1.9$ nm. The solid lines plotted under the profile (c) is a form factor for a cylinder calculated using $r = 16.2$ nm, $\sigma_r = 1.5$ nm. All profiles were corrected for the smearing due to the slit-height and slit-width. In calculating form factors, interfacial thickness was assumed to be infinitely thin.

thermal diffuse scattering arising from the density fluctuations.

3. Results and discussion

3.1. Structural analysis

It is well known that the composition of the A–B diblock copolymer, f (e.g. the volume fraction of block A) controls the equilibrium morphology of the microphase-separated structure in a strong segregation limit [16,24,32–37]. For a nearly symmetric case, i.e. $0.33 < f < 0.67$, lamella structure appears. If the composition of the block copolymer is asymmetric, the spherical structure appears for the A–B block copolymer with $f < 0.17$ (or $f > 0.76$), and the cylindrical structure occurs over the range of $0.17 < f < 0.33$ (or $0.67 < f < 0.76$). Besides these classical structures, some studies reported that bicontinuous structures may appear within a very narrow range of f, i.e. $0.32 < f < 0.35$ (or $0.61 < f < 0.64$) [19,35–40]. According to these conditions, equilibrium structures of the P2VP-b-PI block copolymers used in the present study should exhibit either spherical (P2VP-b-PI (12/88)) or cylindrical (P2VP-b-PI (26/74))

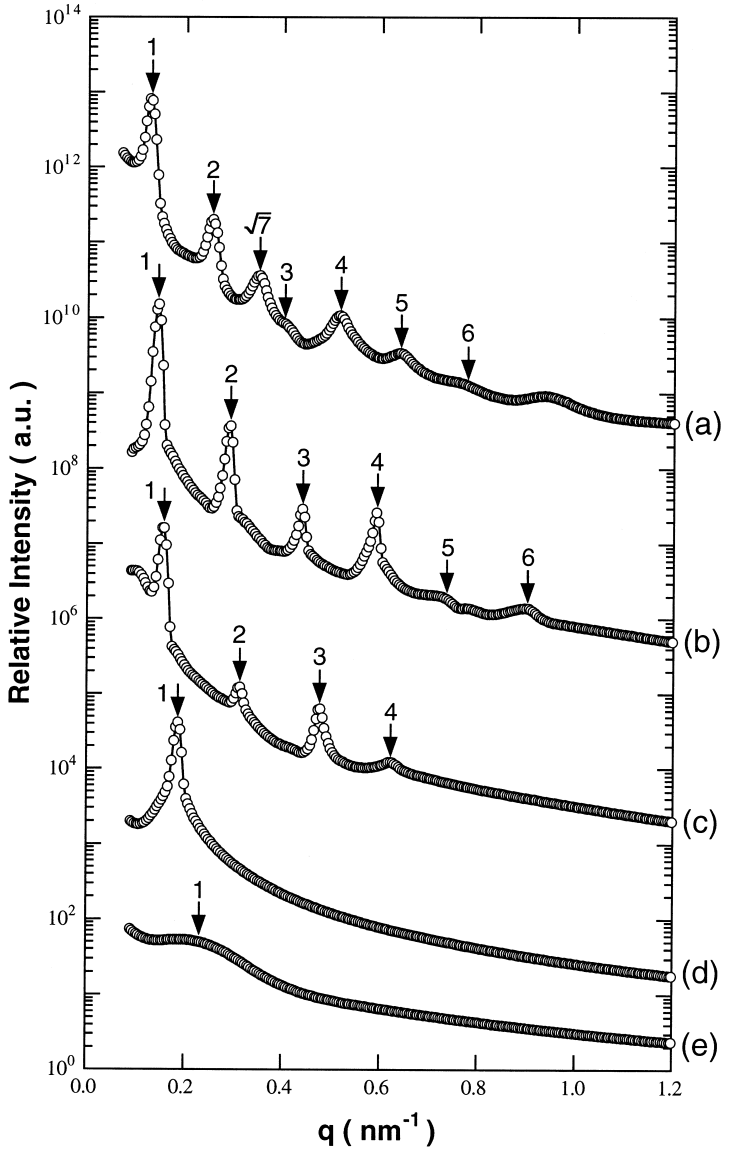

Fig. 3. SAXS profiles for 1,4-dioxane solutions of P2VP-b-PI(26/74) diblock copolymer, at (b) $\phi_p = 57$ wt.%, (c) 43 wt.%, (d) 27 wt.%, and (e) 10 wt.%. Profile (a) is the SAXS profile for the bulk P2VP-b-PI(26/74) film after annealing the as-cast film at 140°C for 12 h. All profiles were corrected for the smearing due to the slit-height and slit-width.

structures (see Table 1). Note that the numbers in the parentheses denote volume percents of the constituents of the block copolymers.

Although the equilibrium morphology can be predicted by the field theories [11–19], the actual structures of the sample films are usually influenced by the way they were prepared. Microphase-separated structures of P2VP-b-PI (26/74) diblock copolymer films obtained by solvent-casting method from (a) *n*-BtCl, (b) CCl_4, (c) toluene, (d) benzene (e) THF, (f) CH_2Cl_2 and (g) 1,4-dioxane solutions were examined by TEM (Fig. 1) and SAXS (Fig. 2). In Fig. 2, SAXS intensity is plotted against a magnitude of scattering vector, **q**, which is defined by $q \equiv |\mathbf{q}| = (4\pi/\lambda)\sin\theta/2$. Here λ and θ are wavelength of X-ray and the scattering angle, respectively. The microphase-separated structures and their domain sizes determined as described in the following paragraphs are summarized in Table 2. Note that the solvents are listed in the order of increasing solubility parameter in Table 2, which will be discussed in Section 3.3.

As seen in Fig. 1(a) and (b), the P2VP-b-PI (26/74) films cast from *n*-BtCl and CCl_4 solutions exhibited disorderly distributed spherical microdomains composed of P2VP blocks in the matrix formed by PI blocks: the bright unstained P2VP spheres exist in the dark PI matrix stained with OsO_4. The corresponding scattering profiles are presented in Fig. 2(a) and (b). We found a single peak marked with a thin arrow labeled "1" due to interparticle interference of the spherical microdomains and three broad peaks marked with thick arrows labeled "1" to "3" which

Table 2
Microphase-separated structures of the cast films determined by SAXS and TEM analyses

Solvent	P2VP-b-PI(26/74)			P2VP-b-PI(12/88)		
	Morphology[a]	Spacing[b] (nm)	Radius[c] (nm)	Morphology[a]	Spacing[b] (nm)	Radius[c] (nm)
n-BtCl	Sphere	34.9	13.9	–	–	–
CCl_4	Sphere	40.7	17.8	Sphere	24.5	8.8
Toluene	Cylinder	47.3	16.2	Sphere	24.9	8.6
Benzene	Cylinder and lamella	48.5	–	–	–	
THF	Cylinder and lamella	48.8	–	Cylinder	35.1	7.8
CH_2Cl_2	Cylinder and lamella	49.0	–	Cylinder	35.2	7.8
1,4-Dioxane	Cylinder and lamella	48.9	–	Cylinder	35.1	7.8

[a] Determined by SAXS and TEM analyses. The sphere and cylinder cores are composed of P2VP block chains.
[b] Average spacing d of the microphase-separated structures was determined from the position of the first-order Bragg diffraction peak q_m in the SAXS profile by using $d = 2\pi/q_m$. Thus the spacing for spherical microdomains in distorted lattice corresponds to the inter-sphere distance, the spacing for hexagonally arranged cylindrical microdomains correspond to the (1 0) plane distance, and the spacing for lamella microdomains correspond to the inter-lamella distance.
[c] Average radius of spherical microdomain was determined by fitting a theoretically calculated form factor to the measured SAXS profile.

are typical for the scattering due to isolated single spherical microdomains (form factor). We have performed theoretical calculations of the form factors whose results are plotted below each profile. The agreements between the theoretical calculations and the actual measurements are found to be satisfactory at large q values, which further confirm that the microphase-separated structures are spherical.

Microphase-separated structure of the P2VP-b-PI (26/74) film obtained form the toluene solution was determined to be cylindrical. In the transmission electron micrograph (Fig. 1(c)), circular cross-sections of bright cylinders composed of P2VP can be found in dark PI matrix. In the corresponding scattering profile (Fig. 2(c)), a typical scattering profile for hexagonally arranged cylinders was found, i.e. the second- and the third-order peaks of the form factor of isolated cylindrical microdomains marked with thick arrows labeled with "2" and "3", and several interference Bragg peaks were observed. The form factor of a cylindrical microdomain is also plotted below the profile, which showed a satisfactory agreement with the profile determined by the actual measurement. The relative positions of the first- and the higher-order Bragg peaks marked with thin arrows were $\sqrt{4}, \sqrt{7}, \sqrt{12}, \sqrt{13}$ which correspond to the Bragg diffraction of (1 0), (2 0), (2 1), (2 2) and (3 1) planes of the hexagonal lattice, respectively. We note that the Bragg peak at relative position of $\sqrt{7}$ is typical for a hexagonal arrangement. It does not appear in scattering profiles of alternating lamellae or spheres arranged in cubic lattices. Thus, existence of the $\sqrt{7}$ Bragg peak can be regarded to evidence of the existence of hexagonally arranged cylinders.

Finally, coexistence of cylindrical and lamellar microdomains were observed in the P2VP-b-PI (26/74) films cast from benzene, THF, CH_2Cl_2 and 1,4-dioxane solutions. In the transmission electron micrographs (Fig. 1(d)–(g)), the coexistence of the regions with stripe-like lamellar microdomains and circular cross-sections of cylindrical microdomain can be clearly observed. The SAXS profiles of these films showed the Bragg interference peak at $\sqrt{7}$ relative to the first-order peak position which is unique for hexagonally arranged cylinders. In addition to these peaks, the scattering peaks at the relative position at 1, 2, 3, 4, 5 and 6 were found, which are typical of lamellar microdomains[1]. Thus the observed SAXS profile can be concluded to be obtained from coexistence of lamellar and cylindrical microdomains whose inter-lamella spacing and (1 0) plane distances are identical.

The morphology of P2VP-b-PI (12/88) block copolymer films determined by SAXS and TEM (micrographs and scattering profiles are not presented) are also listed in Table 2. For this diblock copolymer, the films obtained from CCl_4 and toluene solutions showed spherical microdomain structures, and those cast from THF, CH_2Cl_2 and Dioxane solutions resulted in the cylindrical microdomain structures.

3.2. Evolution of microphase-separated structure in casting process

As shown in Figs. 1 and 2, various microphase-separated structures, such as spherical and cylindrical microdomains

[1] The first- and higher-order Bragg diffraction peaks of hexagonally arranged cylinders appear at the relative positions of $1, \sqrt{3}, \sqrt{4}, \sqrt{7}, \sqrt{9}, \sqrt{12}, \sqrt{13}, \sqrt{16}, \sqrt{19}, \sqrt{21}, \sqrt{25}$ etc. They correspond to the diffraction from (1 0), (1 1), (2 0), (2 1), (3 0), (2 2), (3 1), (4 0), (3 2), (4 1), (5 0) planes, etc., respectively. When the inter-lamellar spacing and the (1 0) plane distance of cylindrical microdomains which are coexisting are identical, $1, \sqrt{4}, \sqrt{9}, \sqrt{16}, \sqrt{25}$ diffraction peaks of the cylindrical microdomains appear at the same positions of the diffraction peaks of the lamellar microdomains. Thus as far as relative peak positions are concerned, differences in the Bragg diffraction profiles of the lamellar and the cylindrical microdomains only appear at $\sqrt{3}, \sqrt{7}, \sqrt{12}, \sqrt{13}, \sqrt{19}$ and $\sqrt{21}$ peaks. The relative peak heights of these depend on volume fraction of the cylindrical domains. The $\sqrt{3}$ peak of the cylinders is sometimes suppressed, depending on the volume fraction of the cylindrical microdomains, which is due to the fact that the form factor of the cylinders becomes a minimum at $\sqrt{3}$ peak of the lattice factor [41]. The $\sqrt{12}$ and $\sqrt{13}$ peaks are easily overlapped and smeared. Moreover, they disappear if the volume fraction of the cylinder is about 0.27. The $\sqrt{19}$ and $\sqrt{21}$ peaks may not be observed if the volume fraction of the cylindrical microdomains is small. These cause only the peak at $\sqrt{7}$ distinguishable as observed in Fig. 2(d)–(g).

as well as the lamella–cylinder coexisting structure, were observed even though the as-cast films were annealed at 140°C for 12 h before the TEM and SAXS observation. Likewise, spherical and cylindrical structures were observed for the films of P2VP-b-PI (12/88). The variation of the structures observed in the film samples may be due to differences in the interaction between the solvent and the two block chains, P2VP and PI. Especially important is the solvent selectivity to one of the two blocks, which affects the effective volumes of each microdomain phase swollen by the solvent. Moreover, the effective volumes change as the solvent evaporates, which may generally induce morphological change during the solvent evaporation.

Thus, to investigate the structural evolution in the process, we have performed the SAXS analyses of the P2VP-b-PI solutions equilibrium at various ϕ_p. In Fig. 3, 1,4-dioxane solutions of the P2VP-b-PI (26/74) at ϕ_ps of (a) 100 wt.% (bulk) after annealing, (b) 57 wt.%, (c) 43 wt.%, (d) 27 wt.% and (e) 10 wt.% are presented. At 10 wt.%, the SAXS profile only exhibited a broad single peak that is due to the correlation hole effect of the disordered block copolymer solution [14,42]. At this ϕ_p, the solution was in the one phase state. At $\phi_p = 27$ wt.%, a distinct sharp interference peak was observed (see Fig. 3(d)), which suggests the existence of the ordered microdomains in the solution. As ϕ_p further increased from 27 to 57 wt.%, a number of the higher-order interference peaks appeared. The relative positions of these peaks with respect to that of the first-order peak were found to be 1, 2, 3, 4, 5 and 6, typical for a lamellar microdomain structure. In this concentration range, no trace of the cylindrical microdomain was found. Finally, after annealing the solvent-cast film, the scattering (Fig. 3(a)) showed the coexistence of lamellar and cylindrical microdomains as was discussed previously. We note that the position of the first peak shifted to a lower q as ϕ_p increased, i.e. the domain spacing increased with increasing the polymer concentration. This tendency can be understood in terms of an increase in the segregation between PI and P2VP blocks with increasing ϕ_p [9,27,43].

As shown in Fig. 3, the microphase-separated structure was already formed in the solution. This structure remained as a non-equilibrium structure in the bulk film obtained after complete solvent evaporation. It is thus very likely that the partition of the solvent in the microdomains developed in the solution plays a significant role, because it changes the "effective" volume ratio of the microdomains. This partition of the solvent makes the microphase-separated structure to be modified from the equilibrium structure in bulk which can be expected from the intrinsic composition of P2VP-b-PI.

P2VP-b-PI (26/74) in dioxane showed lamella structure at polymer concentration up to $\phi_p = 57$ wt.%, presumably because a larger amount of dioxane was partitioned more into the P2VP microdomain (see Fig. 3 and Section 3.3 for details) than into the PI microdomain: The effective volume of the P2VP domains in the solution were larger than f_{P2VP} in bulk. Annealing of the specimen at 140°C for 12 h showed that the cylindrical microdomain appeared but the phase-separated structure did not completely transform from lamella to cylinder (see Fig. 3(a)). The scattering profile did not significantly change after much extensive annealing at 180°C for 72 h. Polystyrene-*block*-polyisoprene (PS-b-PI) would attain equilibrium structures after such prolonged annealing [31]. This difference in the annealing effect on the morphological change may be interpreted as follows: the segregation power defined by a product of the Flory's segmental interaction parameter, χ, and the total degree of polymerization of the block copolymer, N, is larger for P2VP-b-PI than for PS-b-PI by an order of magnitude.[2] Therefore, reorganization of morphology which involves mutual diffusion of the P2VP-b-PI block copolymer molecules, especially across the (lamella) interface, is significantly slower than the PS-b-PI copolymers: The annealing treatment sufficient for equilibrating the PS-b-PI block copolymer is not enough for P2VP-b-PI. Consequently, the nonequilibrium microphase-separated structures developed from various solvents were maintained in the as-cast and even annealed films, demonstrating that the phase-separated structures in solution are important to understand the formation of the structures shown in Table 2.

3.3. Solvent–polymer interaction

Affinity of solvents to polymers can be estimated by introducing the "solubility parameter", δ, which is defined as the square root of the cohesive energy density and describes the strength of attractive force between molecules [44]. In the classical lattice model [45], χ parameter between a polymer and a solvent can be written in terms of δ;

$$\chi = \frac{V_{\text{solvent}}}{RT}\left(\delta_{\text{solvent}} - \delta_{\text{polymer}}\right)^2, \tag{1}$$

where V_{solvent} and R are, respectively, molar volume of the solvent and the gas constant. δ_{solvent} and δ_{polymer} are the solubility parameters of the solvent and the segmental unit of polymer (approximated by 2-vinylpyridine unit or isoprene unit in the present case). The δ mentioned above describes

[2] To the best of our knowledge, there is no report on the χ parameter for P2VP-b-PI. Thus we offer the following estimation. The χ parameter can be roughly estimated by using the relation $d \sim \chi^{1/3}N^{2/3}$ (for lamella), where d is the domain spacing defined by $d = 2\pi/q_m$ (q_m is the wave number where the first-order peak was observed) and N is the degree of polymerization [27]. For P2VP-b-PI, d was evaluated to be $d_{\text{P2VP–PI}} = 47$ nm from the SAXS results for P2VP-b-PI (26/74) obtained from toluene solution as shown in Table 2. Although cylinder was obtained from the toluene solution and thus the above relation does not strictly hold, in the present study, d was not significantly different between lamellar and cylindrical morphology. The d value for the film obtained from a toluene solution was adapted. For the PS-b-PI, d was evaluated to be $d_{\text{PS–PI}} \approx 50$ nm for $N_{\text{PS–PI}} \approx 1200$ ([43], calculated assuming $M_n = 10^5$ ($N = 1200$), $f = 0.5$, $d = 50$ nm and the values are taken from Ref. [10]). Thus, the ratio of χ for P2VP-b-PS, $\chi_{\text{P2VP–PI}}$, and that for PS-b-PI, $\chi_{\text{PS–PI}}$, is estimated to be $\chi_{P2VP–PI}/\chi_{PS–PI} = (d^3_{P2VP–PI}/N^2_{P2VP–PI})/(d^3_{PS–PI}/N^2_{PS–PI}) \sim 8$.

Table 3
Solubility parameters of the solvents and polymers used for the experiments

	$\delta_{solvent}$ (MPa$^{1/2}$)[a]				$\delta_{H,polymer}$ (Mpa$^{1/2}$)
	δ_H[b]	δ_d[b]	δ_p[b]	δ_h[b]	
n-BtCl	17.4	16.4	5.5	2.0	–
CCl_4	17.8	17.8	0.0	0.6	–
Toluene	18.2	18.0	1.4	2.0	–
Benzene	19.4	16.8	5.7	8.0	–
THF	20.3	18.2	6.3	6.1	–
Dioxane	20.5	19.0	1.8	7.4	–
PI	–	–	–	–	16.6[c]
PS	–	–	–	–	18.6[c]
P2VP	–	–	–	–	21.7[d]

[a] Taken from Ref. [48].
[b] δ_d, δ_p, and δ_h are dispersive, polar, and hydrogen bonding terms of the Hansen solubility parameter, respectively.
[c] Taken from Ref. [49].
[d] Assumed to be equal to δ_H for pyridine taken from Ref. [48].

the enthalpy change upon mixing of nonpolar molecules known as Hildebrand solubility parameter [44]. However, as shown in Table 2, some of the solvents used in the present study have permanent dipole (polar solvent). Thus, a modification for δ is required. Hansen [46–48] and Hansen and Skaarup [49] took the following three terms into consideration: dispersive (δ_d), permanent dipole–dipole interaction (δ_p) and hydrogen bonding forces (δ_h),

$$\delta_H^2 = \delta_d^2 + \delta_p^2 + \delta_h^2. \quad (2)$$

The δ_d is related to the London dispersion force. Hansen's solubility parameters, δ_H, for solvents together with $\delta_{H,polymer}$ for PI and P2VP are listed in Table 3. Each of the terms contributing to the Hansen's solubility parameter is also listed in the table. Note that the solubility parameter of P2VP listed in the table is assumed to be equal to that of pyridine, which is used in the following discussion.

The partition of the solvent to the P2VP and PI microdomains is determined by the balance between $(\delta_{H,P2VP} - \delta_{H,solvent})^2$ and $(\delta_{H,PI} - \delta_{H,solvent})^2$, where $\delta_{H,P2VP}$ and $\delta_{H,PI}$ are the Hansen's solubility parameters for P2VP and PI, respectively. If these two quantities are balanced, i.e.

$$(\delta_{H,P2VP} - \delta_{H,solvent})^2 = (\delta_{H,PI} - \delta_{H,solvent})^2 \quad \text{or}$$

$$\delta_{H,solvent} = 1/2(\delta_{H,P2VP} + \delta_{H,PI}) \equiv \delta_{H,neu}, \quad (3)$$

the solvent equally goes to each microdomain ("uniform partition of the solvent"). In this particular case, the solvent acts as a neutral (nonselective) solvent for P2VP-b-PI so that the block copolymer in the solution will attain the equilibrium morphology equal to that for the block copolymer melt, i.e. sphere for P2VP-b-PI (12/88) and cylinder for P2VP-b-PI (26/74).

The morphologies developed in the solvent-cast films will not be equilibrium ones in the bulk, if $\delta_{H,solvent}$ is larger than $\delta_{H,neu}$. As the relation $(\delta_{H,P2VP} - \delta_{H,solvent})^2 < (\delta_{H,PI} - \delta_{H,solvent})^2$ is valid in such cases, the solvents tend to go more to P2VP microdomain rather than PI microdomain. This selective partition of the solvent makes the effective volume ratio of P2VP microdomain to PI microdomain larger than the volume ratio to constituent blocks intrinsic to composition of P2VP, f_{P2VP}. This unequal partition of the solvents modifies the curvature of the interface of the microphase-separated structures in order to attain uniform density distribution of polymer chains over the space, which causes the structures to deviate from the equilibrium in the bulk. In contrast, if $\delta_{H,solvent} < \delta_{H,neu}$ and thus $(\delta_{H,P2VP} - \delta_{H,solvent})^2 > (\delta_{H,PI} - \delta_{H,solvent})^2$, the solvent tends to go more into PI microdomain rather than P2VP microdomain. Hence, for P2VP-b-PI (26/74), the resulting morphology changed from cylinder to sphere upon changing the solvent quality from $\delta_{H,solvent} > \delta_{H,neu}$ to $\delta_{H,solvent} < \delta_{H,neu}$. We note that the structural change did not occur in P2VP-b-PI (12/88) even in the case of $\delta_{H,solvent} < \delta_{H,neu}$, because the sphere, which is the structure observed in the most asymmetric composition, was already attained for the neutral solvent for this copolymer.

Although the P2VP-b-PI (26/74) films cast from toluene solutions showed approximately their equilibrium morphologies, i.e. cylinder, the volume fraction of the cylindrical microdomain turned out to be $0.3 \backsim 0.31$[3]. Since the volume fraction of the P2VP in this block copolymer is 0.26, the cylinder obtained from toluene was not really an equilibrium structure but somewhat swollen. Namely, toluene was partitioned slightly more to the P2VP microdomain than to the PI microdomain in the solution state. Moreover, Benzene, which has a slightly larger value of the Hansen's δ, $\delta_{H,solvent}$, than toluene, gave the coexisting morphology of lamella and cylinder for the solution cast films of P2VP-b-PI (26/74). These facts can be interpreted as a consequence of the solvent being better for P2VP than for PI, and hence the P2VP microdomain was swollen more than the PI microdomain. On the other hand, the P2VP-b-PI (26/74) films cast from CCl_4 solution exhibited the spherical microdomain structure, which means that CCl_4 was better for PI than for P2VP. Therefore, a borderline in terms of δ_H between the equilibrium and the nonequilibrium morphologies for the P2VP-b-PI (26/74) solution-cast films was somewhere between toluene and CCl_4. This border line is consistent with the P2VP-b-PI (12/88), although the morphological change was not observed until δ_H reaches the value of THF. It is rather hard to estimate the neutral solvent from the experimental results obtained from P2VP-b-PI (12/88).

As listed in Table 3, $\delta_{H,P2VP}$ and $\delta_{H,PI}$ values are, respectively, 21.7 and 16.6 MPa$^{1/2}$. According to Eq. (3), therefore, the solubility parameter of the neutral solvent, $\delta_{H,neu}$, is estimated to be 19.1 MPa$^{1/2}$. In contrast, the discussion

[3] Scattering profile from cylindrical structure cast from toluene (profile (c) in Fig. 2) exhibited multiple interference scattering peaks, among which the $\sqrt{3}$ peak was not observed. This feature is realized if the volume fraction of the cylinder is in the range of 0.3 to 0.31 based on the calculation presented in Ref. [41].

presented above suggests that the $\delta_{H,neu}$ lies somewhere between toluene ($\delta_H = 18.2\ MPa^{1/2}$) and CCl_4 ($\delta_H = 17.8\ MPa^{1/2}$): $\delta_{H,neu} \backsim 18\ MPa^{1/2}$. Considering that (1) we discuss only the enthalpic contribution of the solvent partitioning but neglect the entropic contribution due to the uneven partitioning of the solvent and (2) we assumed δ_H of pyridine is equal to that of P2VP, the experimentally estimated $\delta_{H,neu}$, i.e. $18\ MPa^{1/2}$, is in good agreement with the predicted one, i.e. $19\ MPa^{1/2}$.

4. Conclusion

Microphase-separated structures of two P2VP-b-PI copolymers prepared by solvent-casting method using various solvents having a wide range of polarity and degree of hydrogen bonding were studied by transmission electron microscopy (TEM) and small-angle X-ray scattering (SAXS). Two P2VP-b-PI copolymers with different P2VP composition, f_{P2VP}, were examined. Though spherical structure of P2VP is naturally expected for the P2VP-b-PI having $f_{P2VP} = 0.12$ copolymer, cylindrical structure was also observed in some cases. Similarly, besides the cylindrical structure of P2VP, which is expected for P2VP-b-PI having $f_{P2VP} = 0.26$, spherical structure and lamella structure as well as coexisting structure of lamella and cylinder were observed. The various structures reported here are consequences of vitrification of the structures developed during the solvent-casting processes, in which copolymer chains had different radii of gyrations due to polymer–solvent interactions, depending on the solvent used. The formations of the microphase-separated structures were due to the selective partition of the solvent into microphase-separated domains; This was reasonably described by using the Hansen's solubility parameter between the copolymer and the solvent, which incorporates dipole–dipole interaction and hydrogen bonding force in addition to the London dispersion force that is considered in the classical (Hildebrand) solubility parameter.

Acknowledgements

The authors would like to thank Ms. Yuko Kanazawa for help in synthesising the *block* copolymers used in the present study.

References

[1] Hashimoto T, Shibayama M, Fujimura M, Kawai H. In: Meier DJ, editor. Block Copolymers—Science and Technology. London: Haward Academic, 1983. p. 63–108.
[2] Meier DJ. In: Legge NR, Holden G, Schroeder HE, editors. Thermoplastic Elastomers. Munich: Hanser, 1987. chap. 12.
[3] Thomas EL, Alward DB, Henkee CS, Hoffman D. Nature 1988;334:598.
[4] Whitmore MD, Varasour JD. Acta Polymer 1995;46:341 and references therein.
[5] Hasegawa H, Hashimoto T. In: Aggarwal SD, Russo S, editors. Comprehensive Polymer Science, Second Supplement. Oxford: Elsevier Science, 1996. p. 497, chap. 14.
[6] Folkes MJ, Keller A. In: Haward RN, editor. The Physics of Glassy Polymers. London: Applied Science, 1973.
[7] Gallot B. Adv Polym Sci 1978;29:87.
[8] Shibayama M, Hashimoto T, Kawai H. Macromolecules 1983;16:16.
[9] Shibayama M, Hashimoto T, Hasegawa H, Kawai H. Macromolecules 1983;16:1427.
[10] Shibayama M, Hashimoto T, Kawai H. Macromolecules 1983;16:1434.
[11] Meier DJ. J Polym Sci 1969;C26:81.
[12] Helfand E. J Chem Phys 1975;62:999.
[13] Helfand E. J Chem Phys 1975;63:2192.
[14] Leibler L. Macromolecules 1980;13:1602.
[15] Noolandi J, Hong KM. Ferroelectrics 1980;30:117.
[16] Helfand E, Wasserman ZR. In: Goodman I, editor. Developments in Block Copolymers. London: Applied Science, 1982. p. 99–125, chap. 4.
[17] Fredrickson GH, Helfand E. J Chem Phys 1987;87:697.
[18] Fredrickson GH, Leibler L. Macromolecules 1989;22:1238.
[19] Matsen MW, Bates FS. Macromolecules 1996;29:1091.
[20] Hashimoto T, Fujimura M, Kawai H. Macromolecules 1980;13:1660.
[21] Sakurai S, Umeda H, Taie K, Nomura S. J Chem Phys 1996;105:8902.
[22] Fisher E, Henderson JF. Rubber Chem Techno 1967;40:1373.
[23] Inoue T, Soen H, Kawai H, Fukatsu M, Karata M. J Poly Sci B 1968;6:75.
[24] Inoue T, Soen H, Hashimoto T, Kawai H. J Poly Sci A-2 1969;7:1283.
[25] Cohen RE, Bates FS. J Poym Sci Polym Phys Ed 1980;18:2143.
[26] Mori K, Hasegawa H, Hashimoto T. Polymer 1990;31:2638.
[27] Hashimoto T, Shibayama M, Kawai H. Macromolecules 1983;16:1093.
[28] Lodge TP, Hamersky MW, Janley WH, Huang CI. Macromolecules 1997;30:6139.
[29] Matsushita Y, Shimizu K, Nakao Y, Choshi H, Nagasawa M. Polym J 1986;18:361.
[30] Brandrup J, Immergut EH, editors. Polymer Handbook. 3rd ed. New York: Wiley, 1989. Section V.
[31] Schulz M, Khandpur AK, Bates SF, Almdal K, Mortensen K, Hajduk DA, Gruner SM. Macromolecules 1996;29:2857.
[32] Molau GE. In: Aggarwal SL, editor. Block Polymers. New York: Plenum, 1970.
[33] Matsuo M, Sagaye S. In: Molau GE, editor. Colloidal and Morphological Behavior of Block and Graft Copolymers. New York: Plenum, 1971. p. 1.
[34] Hashimoto T, Shibayama M, Fujimura M, Kawai H. Block Copolymers. In: Meier DJ, editor. Science and Technology. London: Harwood Academic Publishers, 1983. p. 63–108.
[35] Thomas EL, Alward DB, Kinning DJ, Martin DC, Handlin Jr DJ, Fetters LJ. Macromolecules 1986;19:2197.
[36] Hasegawa H, Tanaka H, Yamasaki K, Hashimoto T. Macromolecules 1987;20:1651.
[37] Bates FS, Fredrickson GH. Annu Rev Chem 1990;41:525.
[38] Hajduk DA, Harper PE, Gruner SM, Honeker CC, Kim G, Thomas EL, Fetters LJ. Macromolecules 1994;27:4063.
[39] Förster S, Khandpur AK, Zhao J, Bates FS, Hamley IW, Ryan AJ, Bras W. Macromolecules 1994;27:6922.
[40] Laurer JH, Hajduk DA, Fung JC, Sedat JW, Smith SD, Gruner SM, Agard DA, Spontak RJ. Macromolecules 1997;30:3938.
[41] Hashimoto T, Kawamura T, Harada M, Tanaka H. Macromolecules 1994;27:3063.
[42] de Gennes PG. J Phys (Paris) 1970;31:235.
[43] Mori K, Okawara A, Hashimoto T. J Chem Phys 1996;104:7765.

[44] Hildebrand JH, Scott RL. The Solubility of Non-electrolytes. 3rd ed. New York: Reinhold, 1959.
[45] Flory PJ. Principles of Polymer Chemistry. Ithaca: Cornell University Press, 1953.
[46] Hansen CM. Ind Eng Chem Prod Res Dev 1969;8:2.
[47] Hansen CM. J Paint Technol 1967;39:104.
[48] Hansen CM. J Paint Technol 1967;39:505.
[49] Hansen CM, Skaarup K. J Paint Technol 1967;39:511.
[50] Noel C, Monerie I. J Chem Phys Chem Biol 1968;65:2089.